CrossMark

Fatigue Behavior of Ultrafine-Grained 5052 Al Alloy Processed Through Different Rolling Methods

K.K. Yogesha, Amit Joshi, and R. Jayaganthan

In the present study, 5052 Al alloy was processed through different rolling methods to obtain ultrafine grains and its high-cycle fatigue behavior were investigated. The solution-treated Al-Mg alloys (AA 5052) were deformed through different methods such as cryorolling (CR), cryo groove rolling (CGR) and cryo groove rolling followed by warm rolling (CGW), up to 75% thickness reduction. The deformed samples were subjected to mechanical testing such as hardness, tensile and high-cycle fatigue (HCF) test at stress control mode. The CGW samples exhibit better HCF strength when compared to other conditions. The microstructure of the tested samples was characterized by optical microscopy, SEM fractography and TEM to understand the deformation behavior of deformed Al alloy. The improvement in fatigue life of CR and CGR samples is due to effective grain refinement, subgrain formations, and high dislocation density observed in the heavily deformed samples at cryogenic condition as observed from SEM and TEM analysis. However, in case of CGW samples, formation of nanoshear bands accommodates the applied strain during cyclic loading, thereby facilitating dislocation accumulation along with subgrain formations, leading to the high fatigue life. The deformed or broken impurity phase particles found in the deformed samples along with the precipitates that were formed during warm rolling also play a prominent role in enhancing the fatigue strength. These tiny particles hindered the dislocation movement by effectively pinning it at grain boundaries, thereby improving the resistance of crack propagation under cyclic load.

1. Introduction

AA5052 is a medium strength, non-heat treatable alloy and possesses better welding characteristics. Because of its excellent corrosion resistance properties, it is used in both seawater and industrial chemical environments. It exhibits good combination of mechanical properties such as tensile strength and ductility, fatigue strength and fracture toughness.

The fatigue properties of the light alloys are strongly governed by the ultimate tensile strength, which in turn depends on grain size of the materials, as described by Hall-Petch (Ref [1], [2]). There are several mechanical routes to produce ultrafine grain (grain size between 100 and 1000 nm) materials using severe plastic deformation techniques such as high-pressure torsion (HPT) (Ref [3-7]), equi-channel angular pressing (ECAP) (Ref [8-12]), multi-axial forging (MAF) (Ref [13-17]), accumulative roll bonding (ARB) (Ref [18-22]) and repetitive corrugation and straightening (RCS) (Ref [14], [23-26]) to improve its tensile and fracture properties.

P. S. Rao et al. have obtained ultrafine-grained (UFG) Al-7.5Mg by cryomilling and compared its fatigue crack growth rate with larger grained Al-7Mg obtained by powder metallurgy and ingot metallurgy routes. The fatigue crack growth rate in UFG Al-Mg samples is higher than the larger grained Al-7Mg samples as reported in their work. This improvement was attributed to smoother fracture surface morphology in the UFG samples, which closes the crack and deflects it too (Ref [27]).

A. Vinogradov et al. have ECAPed four different Al-Mg-Sc-Zr alloys (Al-6Mg-0.2Sc-0.15zr, Al-4.5Mg-0.2Sc-0.2Zr, Al-3Mg-0.2Sc-0.18Zr and Al-1.5Mg-0.2Sc-0.2Zr) at different temperatures and investigated both high-cycle and low-cycle fatigue properties. It was reported in their work that the fatigue strength has increased with increasing ultimate tensile strength and percentage of Mg content in the alloy (Ref [28]).

In another study of their work, 5056 Al-Mg alloy was ECAPed at 423 K and its fatigue investigations have shown a slight improvement in fatigue life at low stress amplitudes. They also observed that the crack growth rate at relatively small stress intensity factor range (ΔK) is greater in ECAPed material than its bulk counterpart, as crack propagates in a straight line manner with small deviation in ECAPed material, whereas it moves in a zig-zag manner in its bulk alloy, because of its coarse grain structure (Ref [29]).

V. Patlan et al. have performed ECAP of 5056 Al-Mg alloy and short-annealed at 150 °C for 15 min and studied the fatigue performance. They have observed that the ECAP + short-annealed samples exhibit double the tensile elongation than ECAPed samples. It showed better low-cycle fatigue strength during constant strain amplitude, due to grain refinement and the work hardening in the material (Ref [30]). J. H. Cha et al. have ECAPed 5052 Al-Mg alloy with subsequent annealing at 150 °C for 1 h and conducted its low-cycle fatigue test at constant total strain amplitudes of 0.5, 0.7, 0.9 and 1.1%. They

K.K. Yogesha and **Amit Joshi**, Department of Metallurgical and Materials Engineering, Centre of Nanotechnology, Indian Institute of Technology Roorkee, Roorkee 247667, India; and **R. Jayaganthan**, Department of Metallurgical and Materials Engineering, Centre of Nanotechnology, Indian Institute of Technology Roorkee, Roorkee 247667, India; and Department of Engineering Design, Indian Institute of Technology Madras, Chennai 600036, India. Contact e-mails: rjayafmt@iitr.ernet.in and metarj@iitm.ac.in.

observed only cyclic hardening in the ST samples, with the number of fatigue cycles increased at all strain amplitudes, whereas the ECAP-processed samples exhibit cyclic hardening in the beginning and then with saturation till fracture. Also, they observed higher plastic strain in ST samples after a certain number of fatigue cycles as compared to ECAPed ones (Ref 31).

P. Cavaliere et al. have produced ultrafine grains of pure aluminum and pure copper by ECAP at room temperature with twelve and four passes, respectively, using Bc route. They have investigated pure titanium grade-2 ECAPed at 425 °C and pure nickel at 750 °C with eight passes each to produce UFG structures in the alloy. Further, they conducted tensile and fatigue test of the processed samples with load ratio $R = 0.25$ for fatigue test. They observed that the grain refinement through ECAP improves the fatigue properties of the processed samples under stress control mode (Ref 1).

G. Khatibi et al. have performed HPT of commercial pure copper and compared its high-cycle fatigue behavior with conventional grain (CG)-sized copper and ECAP-processed copper. The HPT-processed samples showed better fatigue performance than ECAP-processed samples due to higher stability of extreme fine microstructure ensured by impurities that avoids cyclic-induced recrystallization and grain coarsening (Ref 32).

The cryorolling (CR) has been identified as a potential route to obtain ultrafine grain (UFG) and requires less true strain of order 2-3 as compared to ECAP route (Ref 33, 34).

S. Malekjani et al. have cryorolled and aged (naturally and artificially) 2024 Al alloy to study its cyclic deformation behavior under strain control mode. They have observed that the fatigue performance of artificially aged samples was higher than the naturally aged samples. This was due to decrease in coherency of the precipitates which leads to homogenous deformation in artificially aged samples (Ref 35).

D. Singh et al. have studied the high-cycle fatigue behavior of 5083 Al alloy processed through cryorolling and cryorolling followed by warm rolling. They have observed that the cryorolling followed by warm rolling samples exhibited better fatigue strength than the ST and CR samples. They have reported that the enhancement of fatigue strength in CR samples was attributed to static strength improvement, whereas the improvement in cryorolling followed by warm rolling was due to enhancement in yield strength of the material through various strengthening mechanism like solid solution strengthening, dislocation strengthening, grain boundary strengthening

Table 1 Compositional details AA 5052

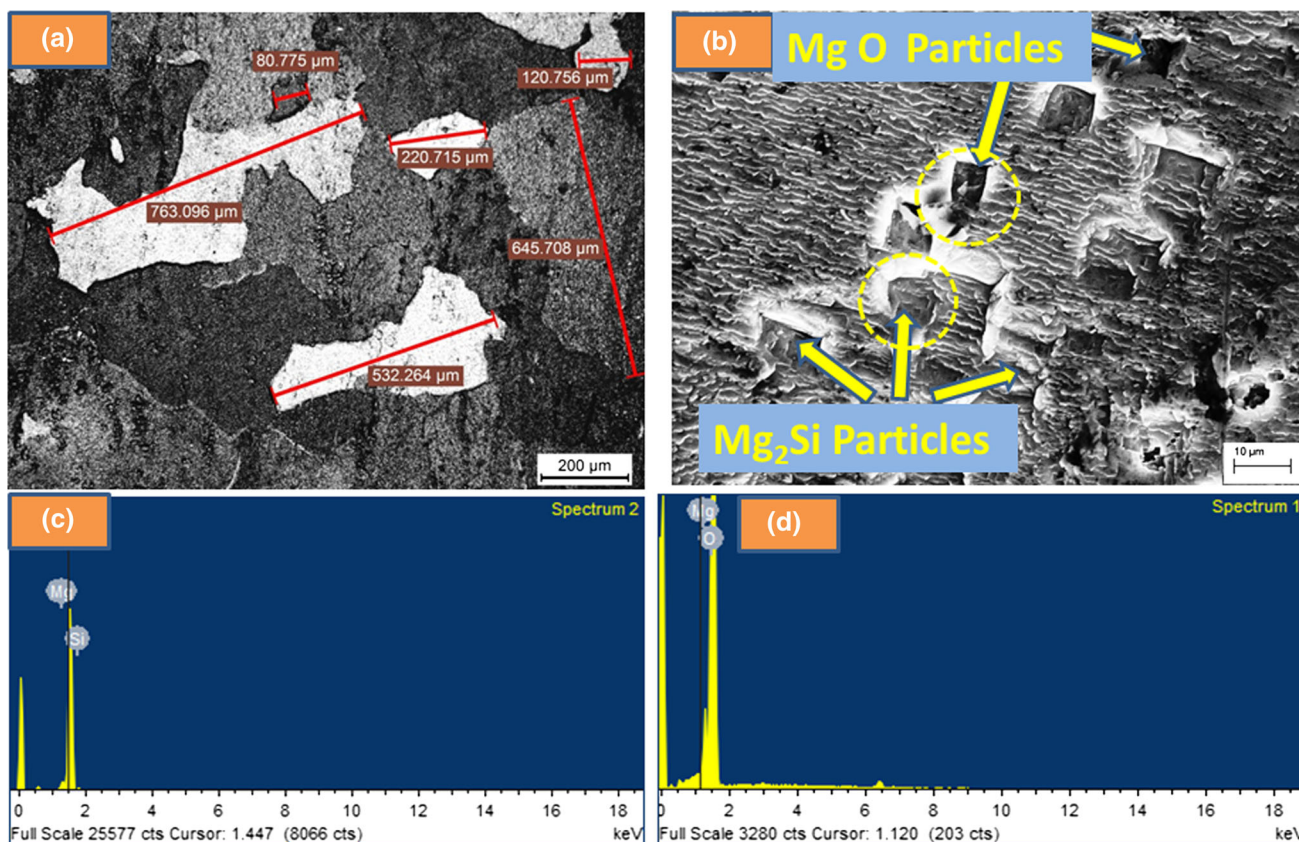| Element	Si	Fe	Cu	Mn	Mg	Cr	Zn	Al
Composition, wt.%	0.20	0.33	0.10	0.10	2.3	0.26	0.10	Remainder

Fig. 1 Optical and SEM images of ST sample with EDS: (a) optical image, (b) high-magnification SEM image, (c) EDS of Mg_2Si particle shown in (b) and (d) EDS of Mg O particle shown in (b)
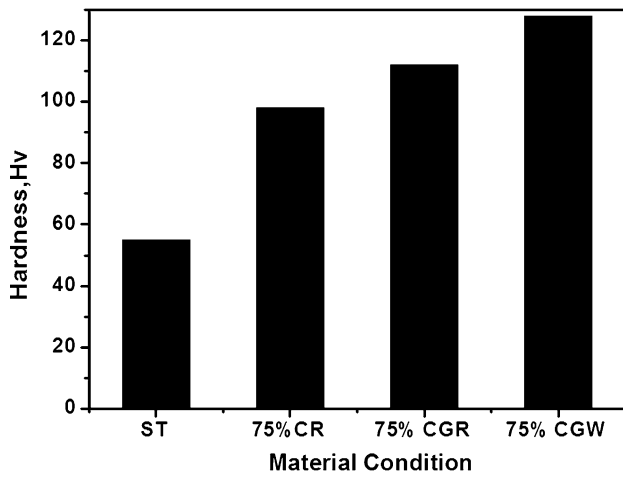
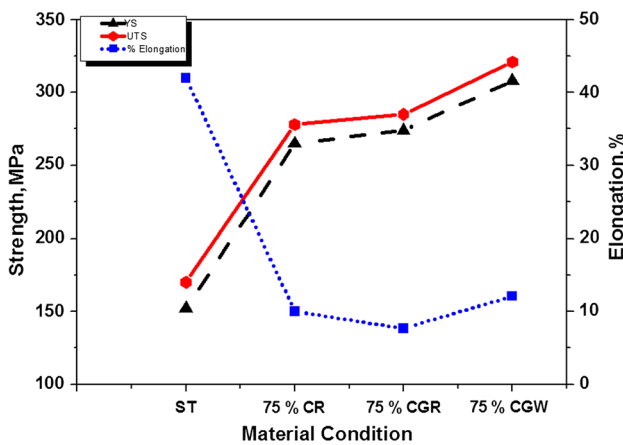**Fig. 2** Variation in hardness with respect to different rolling conditions

Fig. 3 Variation in UTS, YS and percentage elongation of 75% CR-, 75% CGR- and 75% CGW-processed samples
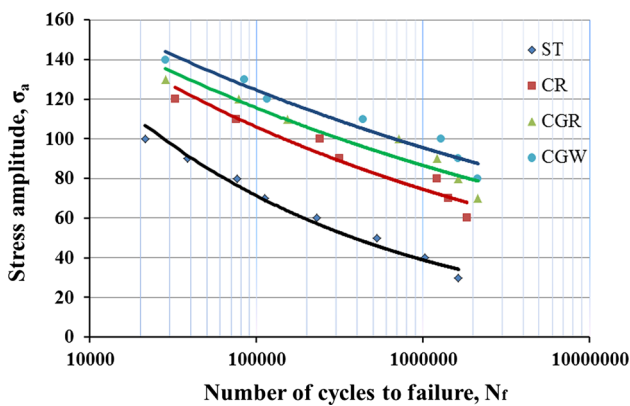

Fig. 4 Stress amplitude vs. number of cycles to failure (*S-N*) behavior of AA 5052 before and after different rolling process

Table 2   Variation of elastic strain component of AA 5052 with fatigue strength after different deformation conditions

Material condition	σ_f, MPa	$\frac{\Delta\varepsilon_{el}}{2}$(a)	N_f(a)
ST	40	0.001085	230,642
CR	75	0.000785	1,218,308
CGR	85	0.000742	1,632,431
CGW	95	0.000704	2,134,421

(a) For a common stress amplitude 80 MPa in all conditions

rolling has been investigated in detail for high cyclic fatigue properties as the deformation is achieved through combined compressive and shear stress.

2. Experimental

2.1 Processing

The commercially available 5052 Al alloy was procured from Vijay Prakash Aeromarine Metals Pvt Ltd, New Delhi, with chemical composition 2.3 wt.% Mg, 0.26 wt.% Cr, 0.2 wt.% Si, 0.33 wt.% Fe, 0.10 wt.% Cu, 0.10 wt.% Mn, 0.10 wt.% Zn and rest aluminum (Table 1). The samples were prepared from the received material to the dimension $60 \times 80 \times 24$ mm and solution-treated (ST) at 540 °C for 2 h followed by water quenching. The ST samples were subjected to grain refinement through different rolling methods. The first set of samples was subjected to cryorolling, where in the samples were rolled in liquid nitrogen atmosphere to achieve effective true strain of 1.38 (75% thickness reduction). The second sets of samples were cryo groove-rolled to an effective true strain of 1.38, where in the samples were groove-rolled (70%) followed by flat rolling (30%) in cryogenic temperature (Ref 35). The homogeneity during the deformation in this step was maintained by reversing the surface (upside down) of the sample after each pass in order to ensure reverse shear deformation. Similarly, the third sets of samples were subjected to cryo groove rolling (70%) followed by warm rolling (30%) at 175 °C to achieve total effective true strain of 1.38. The soaking time for each pass during warm rolling was 5 min.

2.2 Tensile and Hardness Measurements

The deformed samples were subjected to tensile testing and microhardness testing to study the influence of deformation strain on the grain refinement. To perform tensile test, the samples were prepared as per ASTM Standard E-8/E8M-09 subsize with gauge length 25 mm, and test was conducted on Hounsfield universal testing machine model H25K-S with a strain rate of 0.6×10^{-3}/s. The hardness measurement of the deformed samples was performed on Vickers hardness testing machine on plane parallel to the direction of rolling, using a load of 5 kgf with dwell time of 15 s. Each hardness value was determined as a result of ten indentation tests.

2.3 High-Cycle Fatigue Test

The high-cycle fatigue test of all samples was performed on Instron universal testing machine. Fatigue testing samples were

and precipitation strengthening (Ref 36). The present work is focused to investigate fatigue behavior of UFG AA 5052 alloy produced through different rolling techniques such as cryorolling, cryo groove rolling and cryo groove rolling followed by warm rolling and compare the effective grain refinement achieved in each technique. The alloy subjected to cryo groove

prepared by machining the deformed material along the plane of rolling direction as per ASTM E466-15 standards. The sample was polished using emery papers up to 1500 grit size to remove minor surface defects after machining process. The specimens were axially loaded under stress control mode, keeping stress ratio of 0.1 and frequency of 20 Hz in all cases of samples.

The microstructural characterization of all processed samples was conducted by Leica DMI 5000M optical microscope, for which etching of the polished samples was carried out through modified Poulton's reagent. Specimens for TEM characterization were prepared by polishing the deformed and fatigue tested samples up to 80 μm thickness followed by punching it into 3-mm-diameter disks. Twin-jet polishing of these disks was performed in an electrolyte of 10% perchloric

acid and 90% methanol mixture, which is maintained at low temperature of −40 °C, with a DC regulated power supply of 40 V. TEM characterization of these samples was made on FEI Technai TEM instrument.

3. Results and Discussion

3.1 Microstructures

The optical microstructure of ST alloy exhibited equiaxed grain structure with an average grain size of 390 μm is shown in Fig. 1(a). The magnified view of these, which observed through SEM, depicts the presence of impurity phase particles
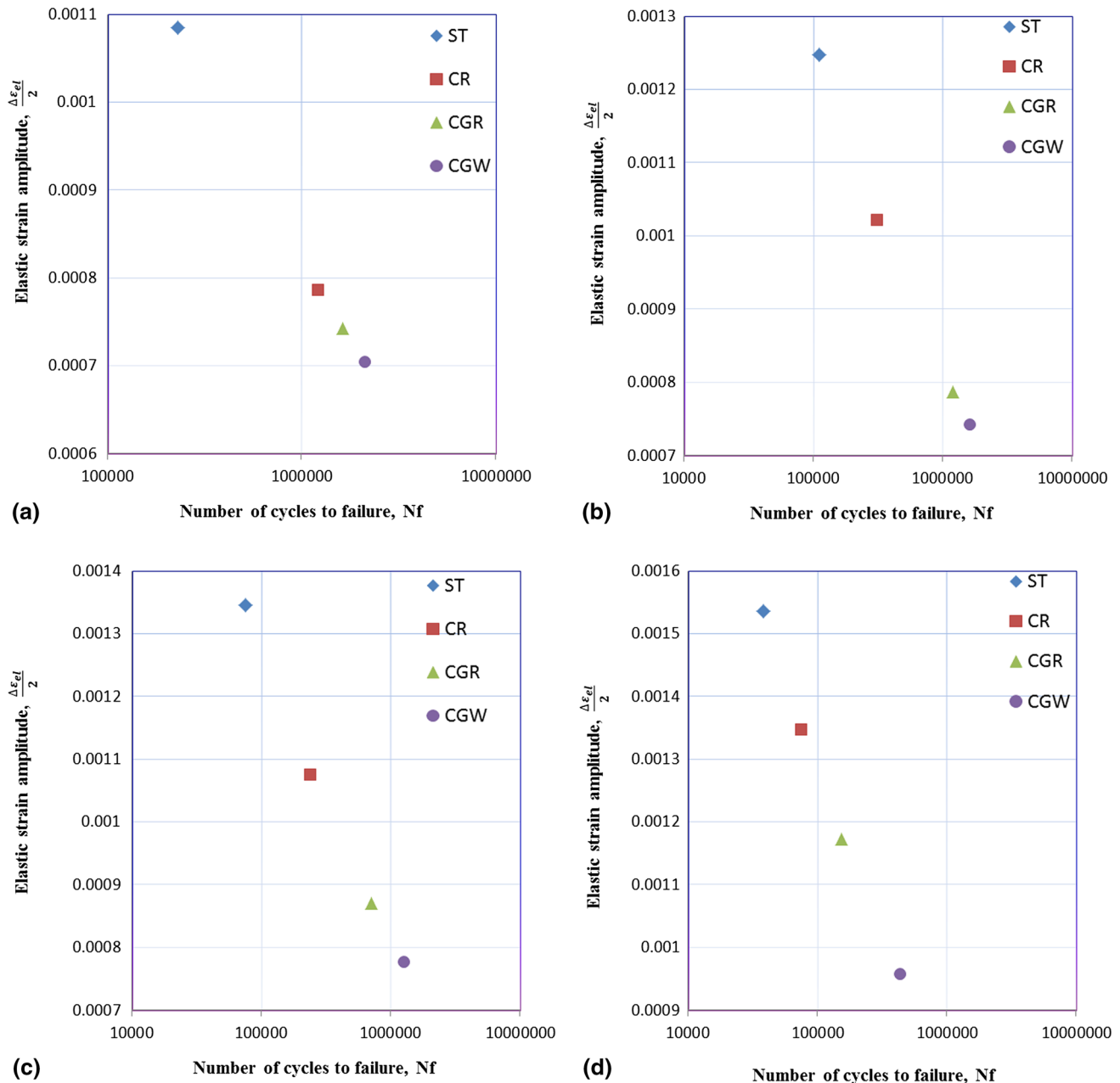

Fig. 5 Variation in elastic strain component vs. number of cycles to failure for different rolling conditions at different stress amplitudes (a) 80 MPa, (b) 90 MPa, (c) 100 MPa and (d) 110 MPa
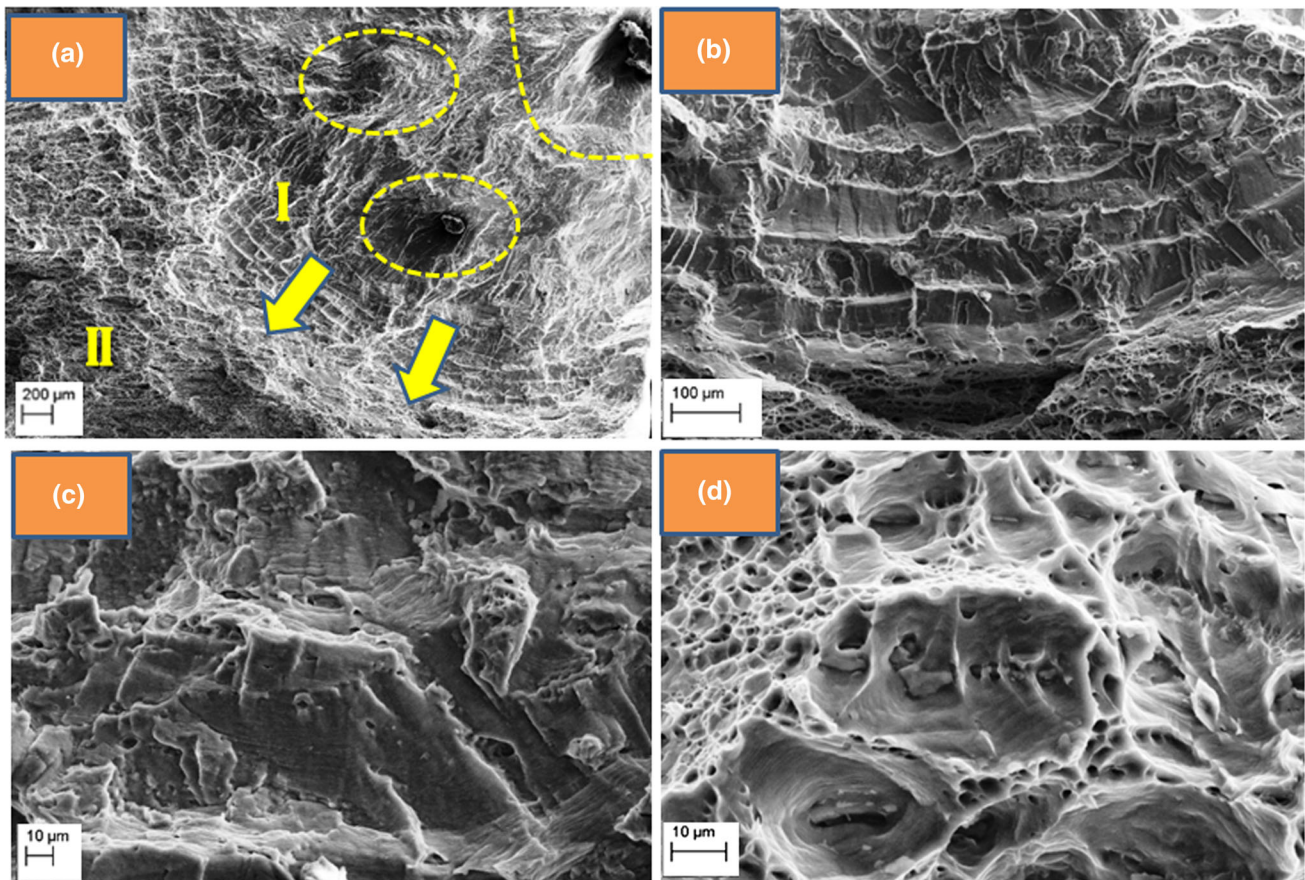
Fig. 6 SEM fractographs of fatigue tested ST sample, (a) low-magnification image showing inclusion sites from where fatigue crack initiates, (b) magnified image of region I with striations, (c) enlarged view of striations, (d) magnified view of region II (fatigue propagation region)

(Mg_2 Si, Mg O) which measures up to 15 µm as shown in Fig. 1(b). These particles are further confirmed with energy-dispersive spectroscopy (EDS) Fig. 1(c) and (d). They promote dislocation accumulation by obstructing the movement of dislocation.

3.2 Tensile and Hardness Properties

Figure 2 shows the variation of strength and ductility of AA5052 with respect to different rolling conditions. The ST samples exhibit UTS of 170 MPa and YS 152 MPa, while its ductility is 42%. The 75% CR and 75% CGR samples possess UTS of 278 and 286 MPa, YS of 265 and 274 MPa, respectively, while their ductility reduced to 10 and 7.7%, respectively. Whereas the 75% CGW samples possess UTS of 321 MPa and YS of 308 MPa, while its ductility increased to 12.1%. Similarly, the hardness values corresponding to ST, CR, CGR and CGW samples are 55, 98, 112 and 128 Hv, respectively (Fig. 3). The increased strength and hardness in CR and CGR samples are attributed to accumulation of high dislocation density during cryogenic process, during which cross-slip or climb associated with dynamic recovery is effectively suppressed (Ref 33, 37, 38). The improved tensile strength, ductility and hardness in CGW sample are due to partial grain refinement and solid solution strengthening (Ref 39, 40). The fine precipitates (Mg_2Al_3) thus formed during warm rolling along with deformed or broken secondary phase impurity particles helps in effective pile up of dislocation movement.

3.3 High-Cycle Fatigue Properties

The stress amplitude (σ_a or S) versus number of cycles to failure (N_f) relation has been plotted (Fig. 4) using experimental data to find out the fatigue strength (σ_f) of each condition.

This fatigue strength or limit is based on 10^6 cycles as a measure of high-cycle fatigue life (Ref 36, 41). Besides grain size, the elastic strain amplitude is more significant for high-cycle fatigue lives, as fatigue strength is directly proportional to strength ($\sigma_f P \sigma_{ut}$).

$$\frac{\Delta_\sigma}{2} = \sigma'_f (2N_f)^b \qquad \text{(Eq 1)}$$

The above Basquin expression which relates stress amplitude to total number of reversal to failure $2N_f$ is used to obtain elastic strain component ($\Delta\varepsilon_{el}$) using the following relation (Ref 1, 28).

$$\frac{\Delta\varepsilon_{el}}{2} = \sigma'_f (2N_f)^b \qquad \text{(Eq 2)}$$

where $\frac{\Delta\varepsilon_{el}}{2} = \frac{\Delta_\sigma}{2E}$, b is Basquin exponent, E is Young's modulus and σ'_f is fatigue strength.

All HCF parameters of processed samples are given in Table 2. A significant improvement in fatigue strength of the processed samples is observed when compared to their ST condition. The samples corresponding to CR and CGR conditions exhibit an increase of 88 and 113% in their fatigue strength, whereas it is 138% in CGW samples as compared to
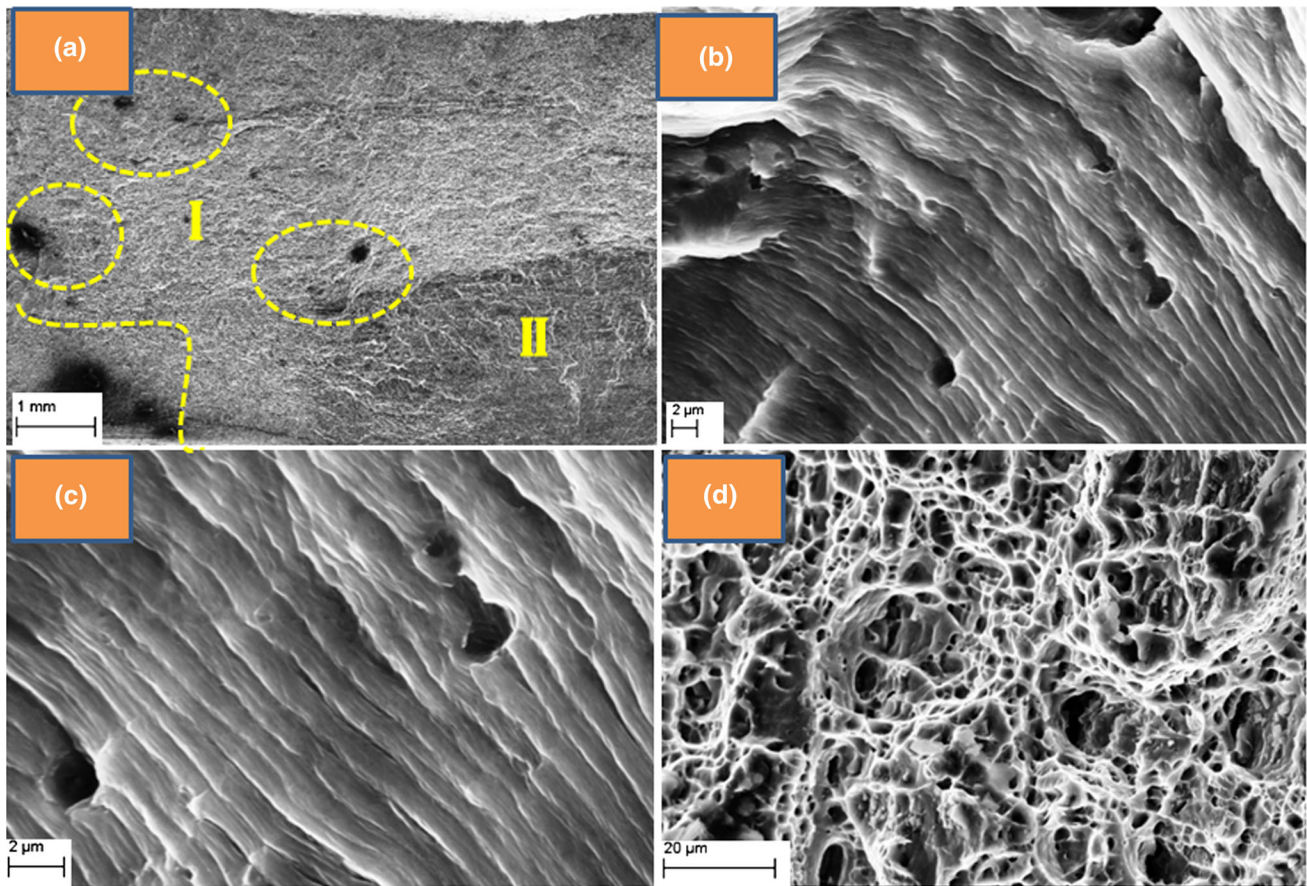
Fig. 7 SEM fractographs of fatigue tested CR sample, (a) low-magnification image showing inclusion sites from where fatigue crack initiates, (b) magnified image of region I with striations, (c) enlarged view of striations, (d) magnified view of region II (fatigue propagation region)

ST samples. On the other hand, the elastic strain component in these processed samples has decreased, least in CGW-processed samples when compared to other processed samples. Figure 5(a), (b), (c) and (d) shows the decreased elastic strain component in samples for the stress amplitude of 80, 90, 100 and 110 MPa.

3.4 Fractographical Analysis of Fatigue Samples

Figures 6, 7, 8, and 9 show the fractured surface of the fatigue tested (at 80 MPa) samples of ST, CR, CGR, CGW conditions, respectively. The mentioned region I and region II in the fractured images represent crack initiation and crack propagation regions, respectively, Fig. 6-9(a). The initiation of cracks in region I occurs at the sites where the Fe-rich inclusions are present. Minimum 2-3 such sites are observed in all the processed condition of samples. Usually, fatigue cracks advance by highly localized plastic rupture, whereas cleavage cracks advance with stepwise growth. Figures 6-9(b) represent magnified view of such region I. Figures 6-9(c) represent striations present in this region, which are similar to ductile striations. The striations are formed as a result of crack propagation at stresses lower than the yield strength. These striations bow out in the direction of crack propagation. The striations gaps are directly linked with the elastic strain component as each of these curved lines represent the position of the crack front during cyclic loading. In ST samples, these striation gaps are measuring around 60 μm. The CR and CGR

samples possess around 1-μm striations gap width, whereas the CGW sample possesses around 0.5 μm gap widths. The magnified views of crack propagation region II are shown in Fig. 6-9(d). Here, the ST samples exhibit large-size dimples and cavities. The CR and CGR samples possess smaller dimples, and the CGR samples possess small amount of cleavage facets over which small dimples are present, which is the reflection of reduced ductility. The CGW samples possess more number of bit bigger dimples compared to CR and CGR samples. Similar kinds of observations were made by Beachem and Yan and Fan while performing fatigue study of 2xxx series Al alloy (Ref 42, 43).

3.5 TEM Analysis

TEM image of the ST sample before the fatigue test is shown in Fig. 10(a), as seen in the optical images, the grains (average size 390 μm) are bigger. The presence of secondary impurity phase particles (MgO, Mg$_2$Si) can be seen in this image. These impurity phase particles were formed during solidification, which are of various shapes like needle, plate and rod. They play a very important role in increasing the strength of the material by obstructing the movement of dislocation through effective pinning at grain boundary (Ref 44-46). Figure 10(a) shows the presence of such particles at the vicinity of grain boundary. Figure 10(b) and (c) shows the TEM images of the CR- and CGR-processed samples, respectively. The images show the density of dislocation imposed and subgrains
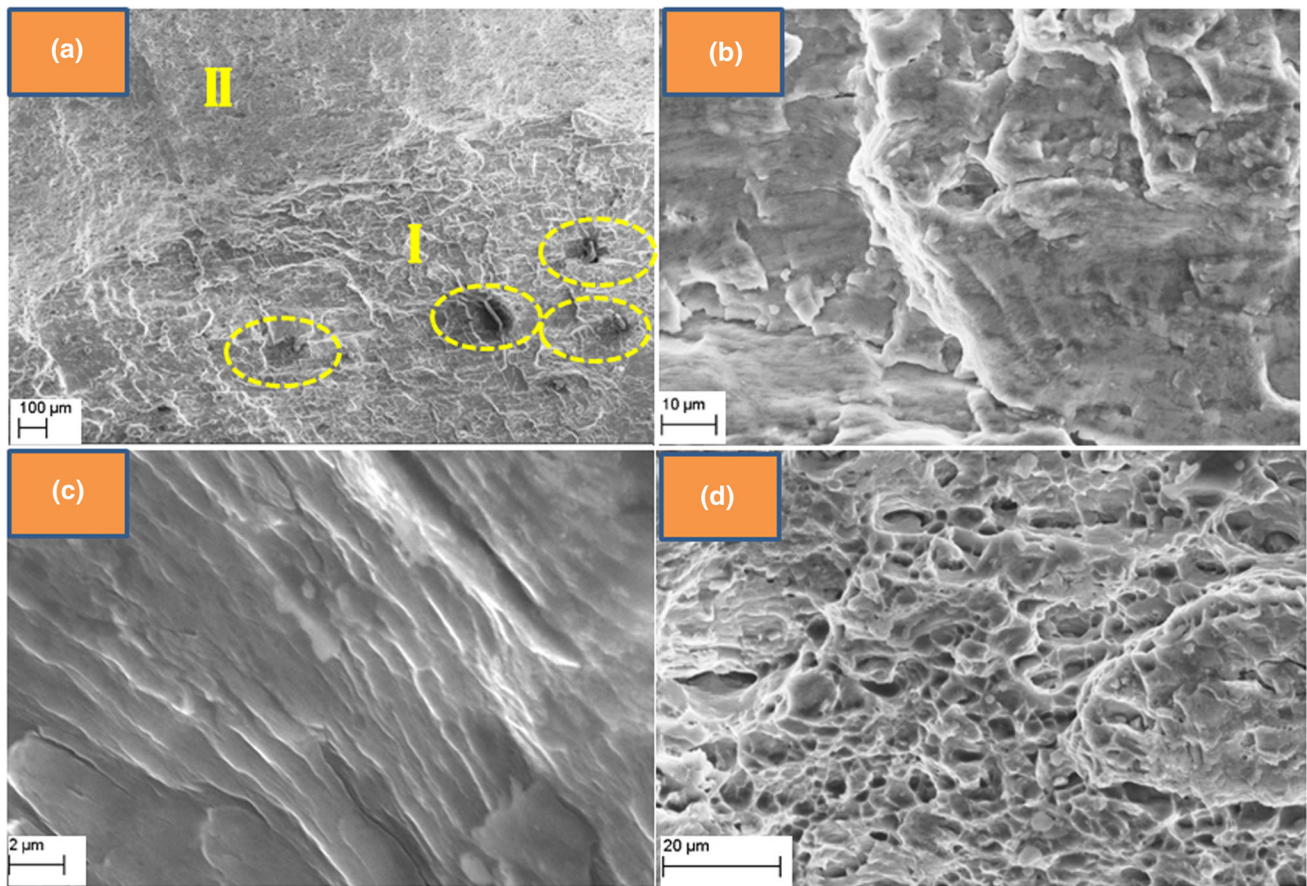
Fig. 8 SEM fractographs of fatigue tested CGR sample, (a) low-magnification image showing inclusion sites from where fatigue crack initiates, (b) magnified image of region I with striations, (c) enlarged view of striations, (d) magnified view of region II (fatigue propagation region)

thus formed during processing. The CGR samples exhibit comparatively higher dislocation density than CR samples; also the subgrains formed in these samples are relatively smaller. The average size of such subgrains in CGR samples is 150 nm, whereas it is 200 nm in CR samples. The CGW sample (Fig. 10d) possesses bit less dislocation density when compared to other processing conditions (CR and CGR) as a result of warm rolling. These samples possess duplex-structured subgrains which include both elongated and equiaxed subgrains with an average subgrain size of 125 nm. The SAED pattern consisting of dotted as well as elongated spots justifies the presence of such subgrains (Fig. 10g), whereas only dotted spots are observed in ST sample (Fig. 10f). The CGR and CGW samples exhibit the formation of nanoshear bands which are layered microstructure formed due to the difference in flow properties of neighboring layers. These bands are formed as a result of intense shear deformation along with compressive deformation in the CGR and CGW process. The magnified image of the CGW sample shows such bands with average band width of 20 nm (Fig. 10e). These shear bands accommodate the applied strain during cyclic loading by prolonging the dislocation accumulation. These are high-energy-stored regions with large orientation gradient in subgrain which makes it favorable for subgrain growth during plastic strain, which enables fatigue strength improvement by delaying crack propagation (Ref 47). Figure 10(f) shows the formation of precipitates (Mg_2Al_3) during warm rolling. These precipitates are around 20- to 50-nm size, which plays a prominent role in

increasing the strength. Singh et al. and Gang et al. have also observed such type of precipitate formation while performing cryorolling followed by warm rolling to improve the strength of Al-Mg alloy through precipitation and dislocation strengthening mechanism (Ref 44, 48). Figure 10(h) shows the presence of deformed or broken impurity phase particles present in alloy after CGW process, which effectively hinders the dislocation movement to increase material strength.

TEM microstructures of the fatigue tested samples, which were obtained at the area nearer crack tip, are shown in Fig. 11. There exists considerable amount of dislocation density over the grains of ST samples due to cyclic loading, during which the interaction between dislocation lines and impurity phase particles support the dislocation pile up (Fig. 11a). The CR and CGR samples possess a small amount of increase in dislocation density; there exists no change in other features Fig. 11(b) and (c). The CGW samples exhibit a considerable increase in dislocation density at some regions Fig. 11(d), the elongated subgrains present, bit stretched and fragmented due to cyclic loading (Fig. 11e). These UFGs are much responsible in increasing the fatigue properties in this stress-controlled mode of tests. The deformed or broken impurity phase particles along with precipitates which were formed during warm rolling are effectively hinder the movement of dislocation, thereby increasing the fatigue strength of the CWG samples as compared to other conditions. Figure 11(f) shows such an impurity phase particle which obstructs the dislocation movement. The EDS of the Mg_2Al_3 precipitates, which were formed
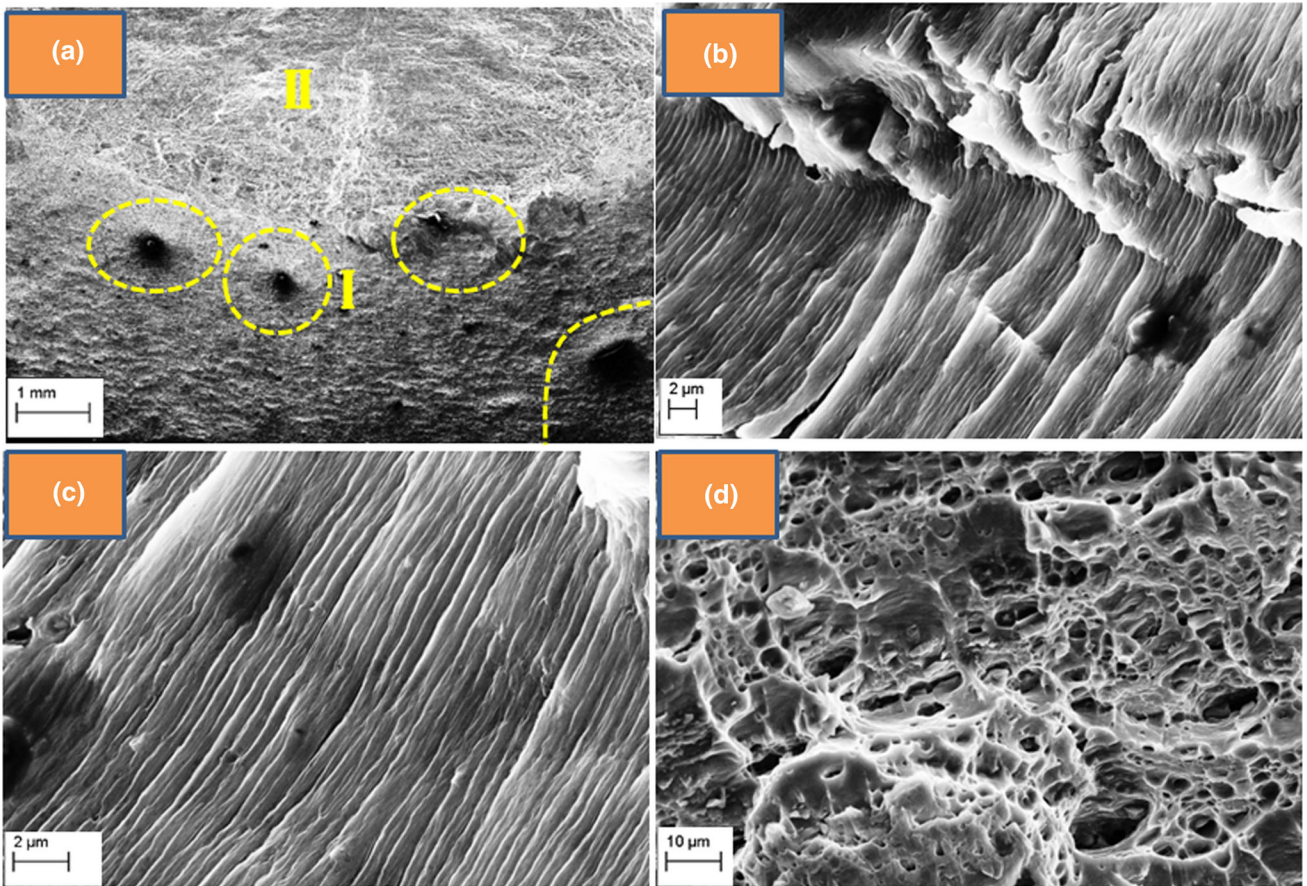
Fig. 9 SEM fractographs of fatigue tested CGW sample, (a) low-magnification image showing inclusion sites from where fatigue crack initiates, (b) magnified image of region I with striations, (c) enlarged view of striations, (d) magnified view of region II (fatigue propagation region)
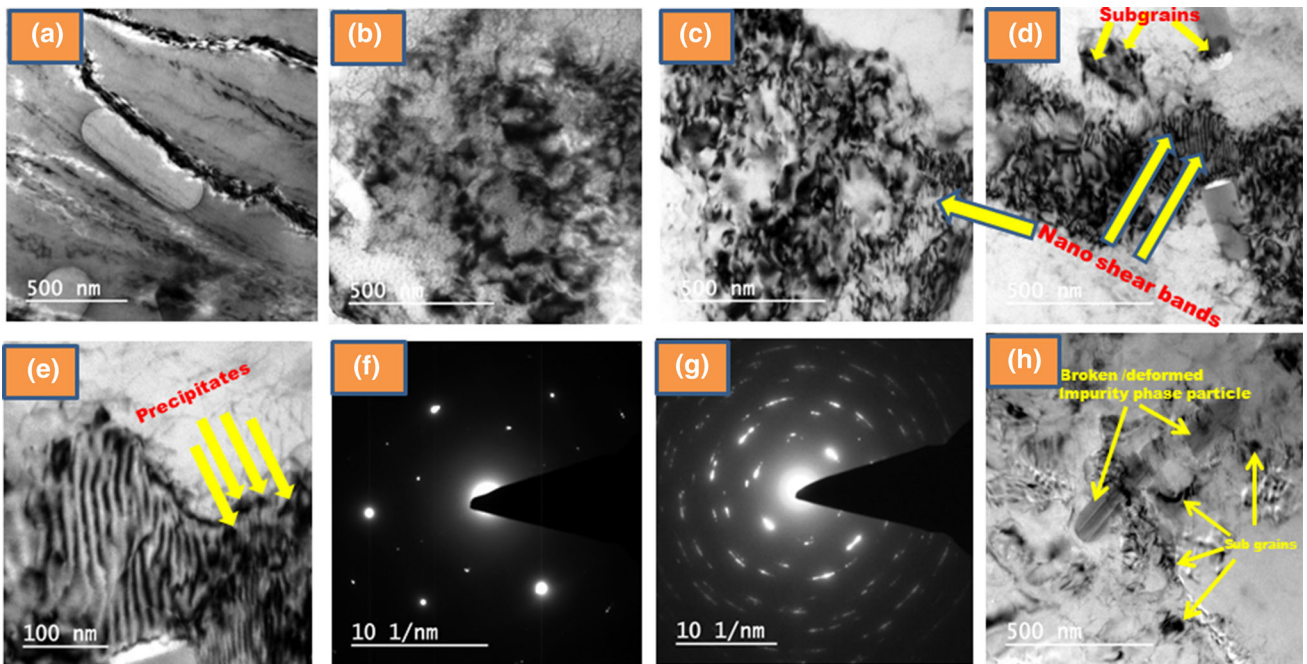

Fig. 10 TEM images AA 5052 after different deformation methods (before fatigue test): (a) ST, (b) 75% CR, (c) 75% CGR, (d) 75% CGW, (e) enlarged view of nanoshear bands with precipitates in 75% CGW specimen, (f) and (g) SAED pattern of ST and CGW specimen, respectively. (h) Deformed or broken impurity phase particle present in CGW specimen
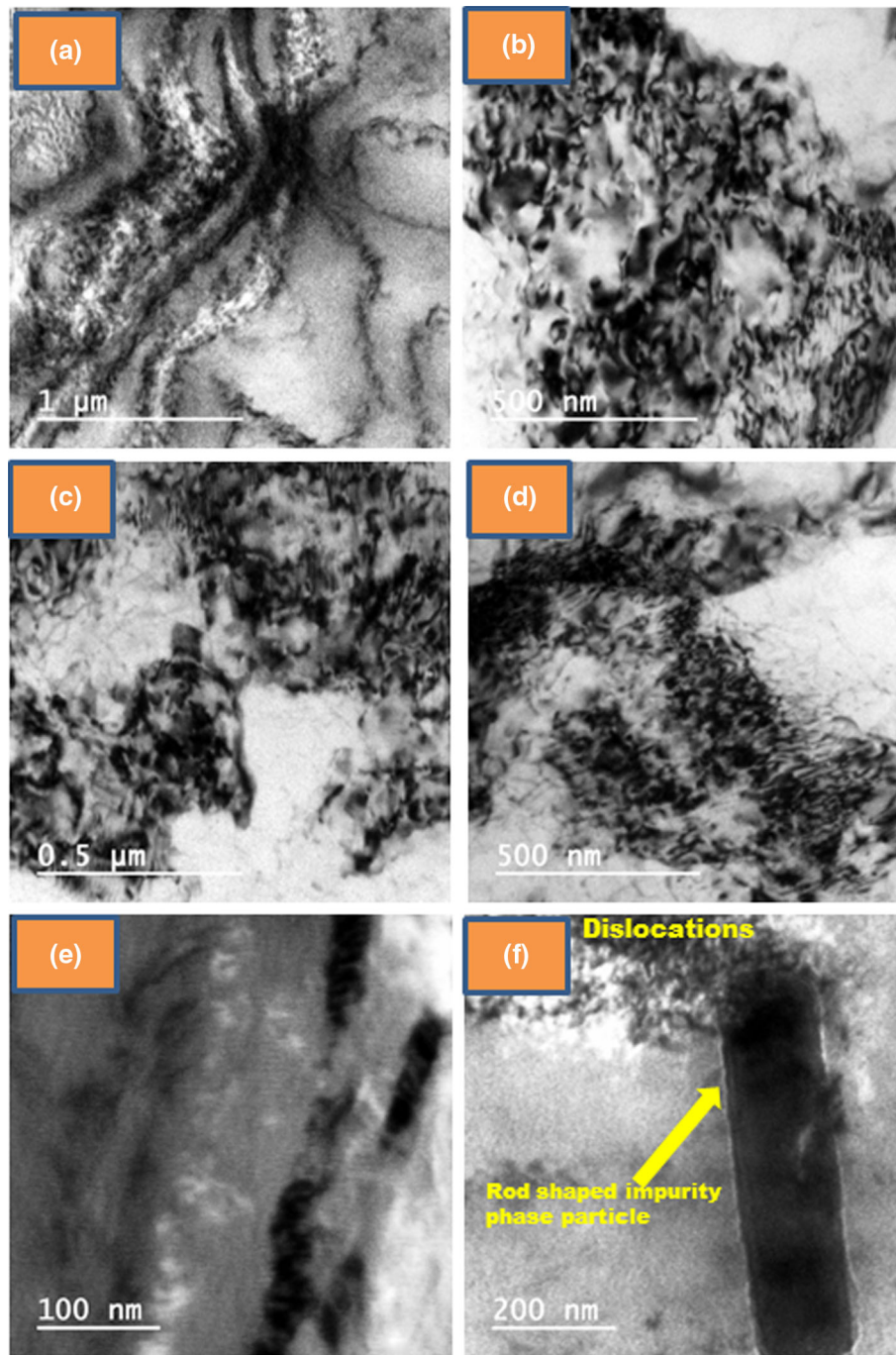
Fig. 11 TEM images AA 5052 (after fatigue test). (a) ST, (b) 75% CR, (c) 75% CGR, (d) 75% CGW, (e) enlarged view of 75% CGW specimen, (f) impurity phase particle hindering the dislocation movement in CGW specimen

during warm rolling of the CGW samples, are shown in Fig. 12.

3.6 XRD Analysis

XRD plot of ST and all deformed samples is shown in Fig. 13. The ST samples show the peaks of α phase Al and impurity phases Mg_2Si, MgO. The CR and CGR samples show the peaks with decreased intensity, revealing the grain refine-ment. The CGW samples show the Mg_2Al_3 peaks, along with Al, Mg_2Si, MgO peaks. The formation of new phase, Mg_2Al_3, is due to the effect of warm rolling during CGW process. These precipitates along with impurity phase particles improve the strength of CGW samples by hindering the dislocation movement effectively as compared to other processed samples. Bo Wang et al. have observed such type of precipitate formation during annealing treatment after conducting cold rolling of 5052 Al alloy (Ref 49).
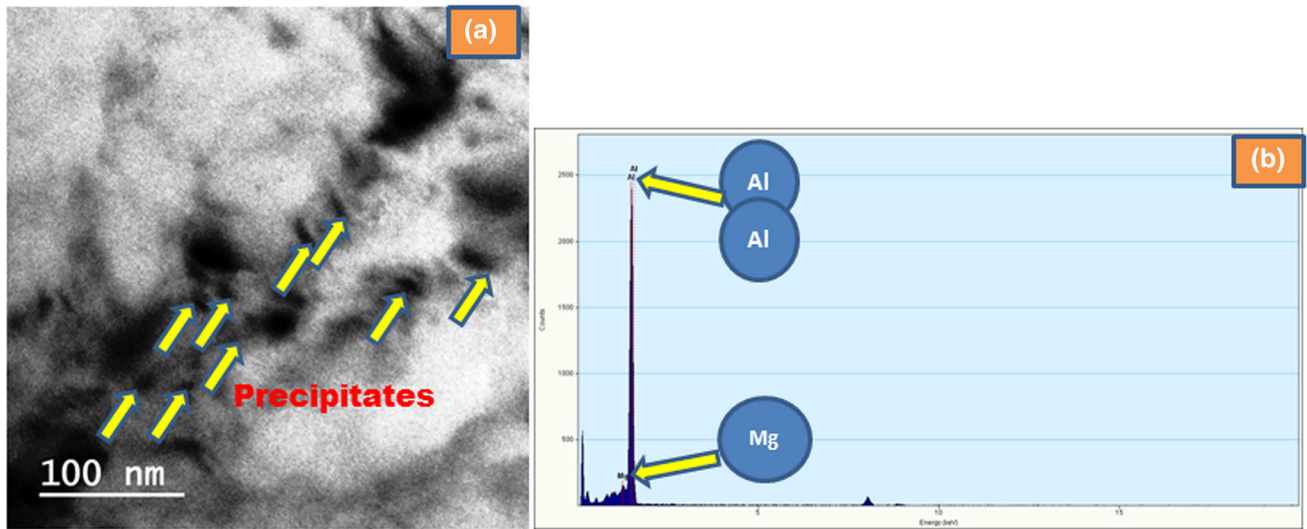
Fig. 12 TEM-EDS of the CGW sample. (a) High-magnification view showing the presence precipitates and (b) EDS of the precipitate particle of (a)
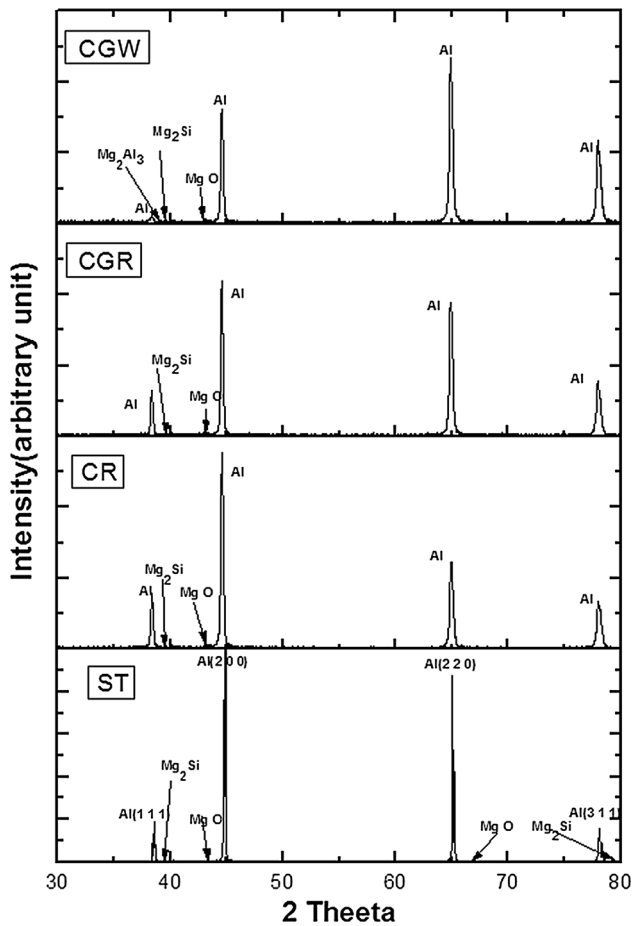

Fig. 13 XRD plot of 5052 Al alloy after different rolling deformation

4. Conclusions

In the present study, the ST 5052 Al alloy has been deformed up to 75% thickness reduction by using different rolling techniques like CR, CGR and CGW process. The fatigue behavior of the processed samples was investigated, and the following conclusions are drawn based on this work.

- CGW samples exhibit comparatively better ultimate tensile strength (321 MPa) and fatigue strength (95 MPa) than CR and CGR samples.
- The presence of subgrains of an average grain size 125 nm in CGW-processed samples plays an important role in increasing the σ_{ut} and σ_f, as grain refinement is responsible in increasing the fatigue properties.
- The formation of nanoshear bands during CGW processing accounts for the improvement in fatigue strength of the Al alloy. It accommodates the applied strain during cyclic loading by prolonging the dislocation accumulation, which delays the crack propagation in the alloy.
- The deformed or broken impurity phase particles present in the CGW samples along with precipitates formed during warm rolling which hinders the dislocation movement also play a prominent role in increasing σ_{ut} and σ_f.
- Very fine striation of width 0.5 µm, as observed in the SEM fractographs of CGW-processed samples, reveals decreased elastic strain component, compared to other conditions.

References

1. P. Cavaliere, Fatigue Properties and Crack Behavior of Ultra-Fine and Nanocrystalline Pure Metals, *Int. J. Fatigue*, 2009, **31**, p 1476–1489
2. N. Hansen, Hall–Petch Relation and Boundary Strengthening, *Scripta Mater.*, 2004, **51**, p 801–806
3. I.F. Mohamed, S. Lee, K. Edalati, Z. Horita, S. Hirosawa, K. Matsuda, and D. Terada, Aging Behavior of Al 6061 Alloy Processed by High-Pressure Torsion and Subsequent Aging, *Metall. Mater. Trans. A*, 2015, **46**, p 2664–2673
4. A.P. Zhilyaev, K. Oh-Ishi, T.G. Langdon, and T.R. McNelley, Microstructural Evolution in Commercial Purity Aluminum During High-Pressure Torsion, *Mater. Sci. Eng. A*, 2005, **410**, p 277–280
5. B.B. Straumal, B. Baretzky, A.A. Mazilkin, F. Phillipp, O.A. Kogtenkova, M.N. Volkov, and R.Z. Valiev, Formation of Nanograined

Structure and Decomposition of Supersaturated Solid Solution During High Pressure Torsion of Al-Zn and Al-Mg Alloys, *Acta Mater.*, 2004, **52**, p 4469–4478

6. X. Yang, J. Yi, S. Ni, Y. Du, and M. Song, Microstructural Evolution and Structure–Hardness Relationship in an Al-4 wt.% Mg Alloy Processed by High-Pressure Torsion, *J. Mater. Eng. Perform.*, 2016, **25**, p 1909–1915

7. C. Xu, Z. Horita, and T.G. Langdon, The Evolution of Homogeneity in an Aluminum Alloy Processed Using High-Pressure Torsion, *Acta Mater.*, 2008, **56**, p 5168–5176

8. Y.H. Zhao, X.Z. Liao, Z. Jin, R.Z. Valiev, and Y.T. Zhu, Microstructures and Mechanical Properties of Ultrafine Grained 7075 Al Alloy Processed by ECAP and Their Evolutions During Annealing, *Acta Mater.*, 2004, **52**, p 4589–4599

9. S.Y. Chang, K.S. Lee, S.H. Choi, and D.H. Shin, Effect of ECAP on Microstructure and Mechanical Properties of a Commercial 6061 Al Alloy Produced by Powder Metallurgy, *J. Alloys Compd.*, 2003, **354**, p 216–220

10. M. Zha, Y. Li, R.H. Mathiesen, R. Bjørge, and H. Roven, J, Microstructure Evolution and Mechanical Behavior of a Binary Al-7Mg Alloy Processed by Equal-Channel Angular Pressing, *Acta Mater.*, 2015, **84**, p 42–54

11. L.J. Zheng, H.X. Li, M.F. Hashmi, C.Q. Chen, Y. Zhang, and M.G. Zeng, Evolution of Microstructure and Strengthening of 7050 Al Alloy by ECAP Combined with Heat-Treatment, *J. Mater. Process. Technol.*, 2006, **171**, p 100–107

12. M. Namdar and S. Jahromi, J, Influence of ECAP on the Fatigue Behavior of Age-Hardenable 2xxx Aluminum Alloy, *Int. J. Miner. Metall. Mater.*, 2015, **22**, p 285–291

13. P.N. Rao, D. Singh, and R. Jayaganthan, Mechanical Properties and Microstructural Evolution of Al 6061 Alloy Processed by Multidirectional Forging at Liquid Nitrogen Temperature, *Mater. Des.*, 2014, **56**, p 97–104

14. R.Z. Valiev, Y. Estrin, Z. Horita, T.G. Langdon, M.J. Zechetbauer, and Y.T. Zhu, Producing bulk Ultrafine-Grained Materials by Severe Plastic Deformation, *JOM*, 2006, **58**, p 33–39

15. O.S. Sitdikov, Comparative Analysis of Microstructures Formed in Highly Alloyed Aluminum Alloy During High-Temperature Equal-Channel Angular Pressing and Multidirectional Forging, *Inorg. Mater. Appl. Res.*, 2016, **7**, p 149–157

16. D. Fuloria, N. Kumar, S. Goel, R. Jayaganthan, S. Jha, and D. Srivastava, Tensile Properties and Microstructural Evolution of Zircaloy-4 Processed Through Rolling at Different Temperatures, *Mater. Des.*, 2016, **103**, p 40–51

17. A. Joshi, N. Kumar, K.K. Yogesha, R. Jayaganthan, and S.K. Nath, Mechanical Properties and Microstructural Evolution in Al 2014 Alloy Processed Through Multidirectional Cryo forging, *J. Mater. Eng. Perform.*, 2016, **25**, p 1–15

18. N. Tsuji, Y. Saito, S.H. Lee, and Y. Minamino, ARB (Accumulative Roll-Bonding) and Other New Techniques to Produce Bulk Ultrafine Grained Materials, *Adv. Eng. Mater.*, 2003, **5**, p 338–344

19. M. Ruppert, M. Strebl, H.W. Höppel, and M. Göken, Mechanical Properties of Ultrafine-Grained AlZnMg (Cu)-Alloys AA7020 and AA7075 Processed by Accumulative Roll Bonding, *J. Mater. Sci.*, 2015, **50**, p 4422–4429

20. H. Xie, M.P. Wang, W. Chen, and Y. Jia, Microstructure, Mechanical Properties, and Texture Evolution of Aluminum Alloy 7005 by Accumulative Roll Bonding, *J. Mater. Eng. Perform.*, 2016, **25**, p 1199–1210

21. H.W. Höppel, J. May, and M. Göken, Enhanced Strength and Ductility in Ultrafine-Grained Aluminium Produced by Accumulative Roll Bonding, *Adv. Eng. Mater.*, 2004, **6**, p 781–784

22. M.Z. Quadir, O. Al-Buhamad, L. Bassman, and M. Ferry, Development of a Recovered/Recrystallized Multilayered Microstructure in Al Alloys by Accumulative Roll Bonding, *Acta Mater.*, 2007, **55**, p 5438–5448

23. J.Y. Huang, Y.T. Zhu, H. Jiang, and T.C. Lowe, Microstructures and Dislocation Configurations in Nanostructured Cu Processed by Repetitive Corrugation and Straightening, *Acta Mater.*, 2001, **49**, p 1497–1505

24. V. Rajinikanth, G. Arora, N. Narasaiah, and K. Venkateswarlu, Effect of Repetitive Corrugation and Straightening on Al and Al–0.25 Sc Alloy, *Mater. Lett.*, 2008, **62**, p 301–304

25. N. Thangapandian, S.B. Prabu, and K.A. Padmanabhan, Effects of Die Profile on Grain Refinement in Al-Mg Alloy Processed by Repetitive Corrugation and Straightening, *Mater. Sci. Eng. A*, 2016, **649**, p 229–238

26. A. Krishnaiah, U. Chakkingal, and H.S. Kim, Mechanical Properties of Commercially Pure Aluminium Subjected to Repetitive Bending and Straightening Process, *Trans. Indian Inst. Met.*, 2008, **61**, p 165–167

27. P.S. Pao, H.N. Jones, S.F. Cheng, and C.R. Feng, Fatigue Crack Propagation in Ultrafine Grained Al-Mg Alloy, *Int. J. Fatigue*, 2005, **27**, p 1164–1169

28. A. Vinogradov, A. Washikita, K. Kitagawa, and V.I. Kopylov, Fatigue life of Fine-Grain Al-Mg-Sc Alloys Produced by Equal-Channel Angular Pressing, *Mater. Sci. Eng. A*, 2003, **349**, p 318–326

29. A. Vinogradov, S. Nagasaki, V. Patlan, K. Kitagawa, and M. Kawazoe, Fatigue Properties of 5056 Al-Mg Alloy Produced by Equal-Channel Angular Pressing, *Nanostruct. Mater.*, 1999, **11**, p 925–934

30. V. Patlan, A. Vinogradov, K. Higashi, and K. Kitagawa, Overview of Fatigue Properties of Fine Grain 5056 Al-Mg Alloy Processed by Equal-Channel Angular Pressing, *Mater. Sci. Eng. A*, 2001, **300**, p 171–182

31. J.H. Cha, H.H. Cho, W.H. Kim, S.I. Kwun, and D.H. Shin, The Low Cycle Fatigue Behavior of Equal-Channel Angular Pressed Al 5052 Alloy, *Key Eng. Mater.*, 2008, **385**, p 725–728

32. G. Khatibi, J. Horky, B. Weiss, and M.J. Zehetbauer, High Cycle Fatigue Behaviour of Copper Deformed by High Pressure Torsion, *Int. J. Fatigue*, 2010, **32**, p 269–278

33. S.K. Panigrahi and R. Jayaganthan, A Study on the Mechanical Properties of Cryorolled Al-Mg-Si Alloy, *Mater. Sci. Eng. A*, 2008, **480**, p 299–305

34. K.K. Yogesha, N. Kumar, A. Joshi, R. Jayaganthan, and S.K. Nath, A Comparative Study on Tensile and Fracture Behavior of Al-Mg Alloy Processed Through Cryorolling and Cryo Groove Rolling, *Metallogr. Microstruct. Anal.*, 2016, **5**, p 251–263

35. S. Malekjani, P.D. Hodgson, P. Cizek, I. Sabirov, and T.B. Hilditch, Cyclic Deformation Response of UFG 2024 Al Alloy, *Int. J. Fatigue*, 2011, **33**(5), p 700–709

36. D. Singh, P. Nageswara Rao, and R. Jayaganthan, High Cyclic Fatigue Behaviour of Ultrafine Grained Al 5083 Alloy, *Mater. Sci. Technol.*, 2014, **30**, p 1835–1842

37. U.G. Kang et al., The Improvement of Strength and Ductility in Ultra-Fine Grained 5052 Al Alloy by Cryogenic-and Warm-Rolling, *J. Mater. Sci.*, 2010, **45**, p 4739–4744

38. Y.B. Lee, D.H. Shin, and W.J. Nam, Effect of Annealing Temperature on Tensile Behavior of 5052 Al Alloy Deformed at Cryogenic Temperature, *J. Mater. Sci.*, 2005, **40**, p 1313–1315

39. P.N. Rao, D. Singh, and R. Jayaganthan, Effect of Annealing on Microstructure and Mechanical Properties of Al 6061 Alloy Processed by Cryorolling, *Mater. Sci. Technol.*, 2013, **29**, p 76–82

40. S.K. Panigrahi and R. Jayaganthan, Development of Ultrafine-Grained Al 6063 Alloy by Cryorolling with the Optimized Initial Heat Treatment Conditions, *Mater. Des.*, 2011, **32**, p 2172–2180

41. T.S. Srivatsan, S. Anand, S. Sriram, and V.K. Vasudevan, The High-Cycle Fatigue and Fracture Behavior of Aluminum Alloy 7055, *Mater. Sci. Eng. A*, 2000, **281**(1), p 292–304

42. C.D. Beachem, Electron Fractographic Studies of Mechanical Fracture Processes in Metals, *J. Basic Eng.*, 1965, **87**, p 299–306

43. L. Yan and J. Fan, In-Situ SEM Study of Fatigue Crack Initiation and Propagation Behavior in 2524 Aluminum Alloy, *Mater. Des.*, 2016, **110**, p 592–601

44. D. Singh, P. Nageswara Rao, and R. Jayaganthan, Effect of Deformation Temperature on Mechanical Properties of Ultrafine Grained Al-Mg Alloys Processed by Rolling, *Mater. Des.*, 2013, **50**, p 646–655

45. A. Gholinia, F.J. Humphreys, and P.B. Prangnell, Production of Ultra-Fine Grain Microstructures in Al-Mg Alloys by Coventional Rolling, *Acta Mater.*, 2002, **50**, p 4461–4476

46. D. Singh, P. Nageswara Rao, and R. Jayaganthan, Microstructures and Impact Toughness Behavior of Al 5083 Alloy Processed by Cryorolling and Afterwards Annealing, *Int. J. Miner. Metall. Mater.*, 2013, **20**, p 759–769

47. S. Malekjani, P.D. Hodgson, N.E. Stanford, and T.B. Hilditch, Shear Bands Evolution in Ultrafine-Grained Aluminium Under Cyclic Loading, *Scripta Mater.*, 2013, **68**(10), p 821–824

48. U.G. Gang, S.H. Lee, and W.J. Nam, The Evolution of Microstructure and Mechanical Properties of a 5052 Aluminium Alloy by the Application of Cryogenic Rolling and Warm Rolling, *Mater. Trans.*, 2009, **50**(1), p 82–86

49. W. Bo, X.H. Chen, F.S. Pan, J.J. Mao, and F.A.N.G. Yong, Effects of Cold Rolling and Heat Treatment on Microstructure and Mechanical Properties of AA 5052 Aluminum Alloy, *Trans. Nonferrous Met. Soc. China*, 2015, **25**(8), p 2481–2489